communications earth & environment

Article

https://doi.org/10.1038/s43247-024-01422-7

Teleconnection of the Quasi-biennial oscillation with boreal winter surface climate in Eurasia and North America

Check for updates

Vinay Kumar [1] ✉, Matthew H. Hitchman[2], Wenyuan Du [2], S. K. Dhaka[1] & Shigeo Yoden[3]

An improved understanding of dynamical coupling from regional to global scales via tropospheric or stratospheric region can be helpful in improving seasonal forecasts for a given region of interest. Here we investigate dynamical coupling between the equatorial stratospheric Quasi-biennial oscillation and the boreal winter surface climate of the Northern Hemisphere mid and high latitudes using 42 years of data (1979–2020). For neutral El Niño Southern Oscillation periods, the Quasi-biennial oscillation westerly phase at 70 hPa favors high sea level pressure in the polar region, colder conditions and deeper snow over Eurasia and North America, and the opposite effects for the easterly phase. When Quasi-biennial oscillation anomalies arrive near the tropopause, it is observed that planetary wave activity is enhanced towards to extratropical region during westerly phase and reduced during easterly phase. This teleconnection pathway via the upper troposphere and lower stratosphere to the high latitude surface is independent of the "stratospheric pathway" (Holton-Tan mechanism). Diagnosis of this pathway can help to improve understanding of sub-seasonal to seasonal variations, and long-range forecasting over Eurasia and North America.

The role of dynamical coupling between the stratosphere and troposphere and between the tropics and extratropics in causing regional climate variations is a topic of increasing interest. The boreal winter (December–January–February [DJF]) is a dynamically active season in the Northern Hemisphere (NH), with the presence of vertically propagating planetary wave activity in stratospheric westerlies[1,2], and more active deep convection in the tropics[3]. In this season, certain kinds of dynamical coupling are possible between the tropical stratosphere and extratropical troposphere. A better understanding of this coupling would benefit the populations of Eurasia and North America with improved winter forecasting, as dynamically modulated by regional and global atmospheric circulations[4,5]. These include the tropospheric El Niño Southern Oscillation (ENSO)[6], with a periodicity of ~3–7 years, and the Quasi-biennial oscillation (QBO)[7], which has a periodicity of 22–34 months and is a dominant mode of interannual variability in the equatorial stratosphere.

ENSO is a tropospheric source of dynamical coupling between tropical and extratropical regions, through modulation of planetary waves in both the troposphere and stratosphere[8,9], and is one of the key ingredients used in forecasting wintertime surface climate anomalies for the NH extratropics[10–14]. ENSO teleconnections can involve both a tropospheric[5] and a stratospheric pathway[13,15]. Butler et al.[15] reasoned that North America is primarily affected via the tropospheric pathway, involving a shift in the Pacific North America pattern, while the surface climate response over large portions of Eurasia, the Arctic, and the North Atlantic are influenced by the stratospheric pathway via modulation of the polar vortex.

Stratosphere forcing can also contribute to the predictability of climate-related extreme events at the surface[16]. The QBO is a dominant equatorial stratospheric dynamical forcing, having broad impacts over the globe[7]. Its inclusion significantly enhances seasonal to decadal forecast systems[17]. Impacts of the QBO have been studied in the tropical and subtropical region involving the direct effect on deep convective systems[18–22], and in the polar region via the polar vortex[23–26]. The QBO dynamical teleconnection has three potential routes of influence, referred to as the tropical, subtropical, and polar routes[21,27]. However, these three routes can be classified into two pathways to separate their responses[21,26–28]. The tropical and subtropical routes are associated with the "tropospheric pathway" along the tropical and subtropical upper troposphere and lower stratosphere (UTLS)[28]. In this pathway, QBO anomalies in mean meridional circulation (MMC), temperature, and zonal wind[28] can interact with synoptic Rossby wave patterns, which can then affect the extratropical troposphere via modulation of the Northern annular mode (NAM)[23]. The polar route is associated with the "stratospheric pathway", where QBO anomalies of MMC, temperature, and

[1]Radio and Atmospheric Physics Lab., Rajdhani College, University of Delhi, Delhi, India. [2]Department of Atmospheric and Oceanic Sciences, University of Wisconsin–Madison, Madison, WI, USA. [3]Institute for Liberal Arts and Sciences, Kyoto University, Kyoto, Japan. ✉e-mail: dabas.vinay@gmail.com

zonal wind in the subtropical stratosphere modulate stratospheric planetary wave absorption (Holton-Tan mechanism or "H-T effect")[29,30].

Holton and Tan[29,30] showed that sudden stratospheric warmings (SSWs) occur more often when there are QBO easterly (E) in the tropical stratosphere near 50 hPa. In turn, SSWs are related to an increase in negative phases of the NAM and Arctic oscillation (AO)[31] in sea level pressure, and more cold air outbreaks at the surface in North America and Eurasia[31,32]. The "H-T effect" is an example of the stratospheric pathway from the tropical stratosphere to the extratropical surface. It has also been observed that ENSO modulates the QBO MMC[26,28], QBO amplitude[33], and QBO period via modulation of its downward propagation speed[33–35]. Further, both modeling[36] and observational studies[26,37] have shown that the interaction between different phases of ENSO and the QBO produces a nonlinear effect in the QBO dynamical teleconnection. Hasen et al.[36] showed that QBO anomalies extend down to the troposphere most significantly during La Niña. Observational studies[26,37] found that La Niña amplifies the QBO dynamical teleconnection to the polar vortex, thereby influencing the stratospheric pathway. Kumar et al.[26] also found that La Niña (El Niño) tends to amplify (nullify) the QBO MMC in the winter hemisphere. Recently, ref. 38 pointed out that QBO teleconnections to the subtropics are more evident during El Niño winters, while teleconnections to the polar regions are more evident during La Niña winters. ENSO influences both the tropospheric and stratospheric pathways. It is, therefore, important to investigate each combined ENSO and QBO state in order to understand QBO teleconnections.

As mentioned above, in past studies, the influence of the QBO on the high latitude boreal winter surface climate was discussed in terms of modulation of polar vortex intensity[27,39,40]. However, a complete dynamical mechanism for downward coupling is yet to be established[41]. Until now, QBO winter teleconnections to the surface have been reproduced in models with mixed success, and current QBO forecast biases highlight model deficiencies needing future improvement[42]. Updated observational studies will play a crucial role in such improvements. Most of these studies used a single level for the QBO index, either 30, 50, or 70 hPa, and considered two phases of the QBO, westerly and easterly, irrespective of ENSO phases. However, the QBO varies continuously in phase, with a distinct pattern of temperature and wind anomalies associated with the QBO MMC that descend in time such that any one point experiences a sinusoidal range of phases (see, e.g., Fig.1 and 21 of ref. 28). In the present work we define QBO phase using empirical orthogonal function (EOF) analysis, which includes phase information over a wider range of altitudes than a single level index. The method of ref. 43 is adopted to define the QBO phase angle. Here, we seek to identify a QBO—surface weather climate linkage using composite differences between opposite phase angles of the QBO in the most recent European Centre for Medium-Range Weather Forecasts (ECMWF) Reanalysis v5 (ERA-5) data set from the satellite era 1979–2020. As discussed above the role of ENSO is important in determining the boreal winter surface climate as well as influencing QBO dynamical teleconnection. In this work, the joint effects of the ENSO and QBO are discerned in a systematic fashion using a phase sweep of the QBO phase angle. This allows for

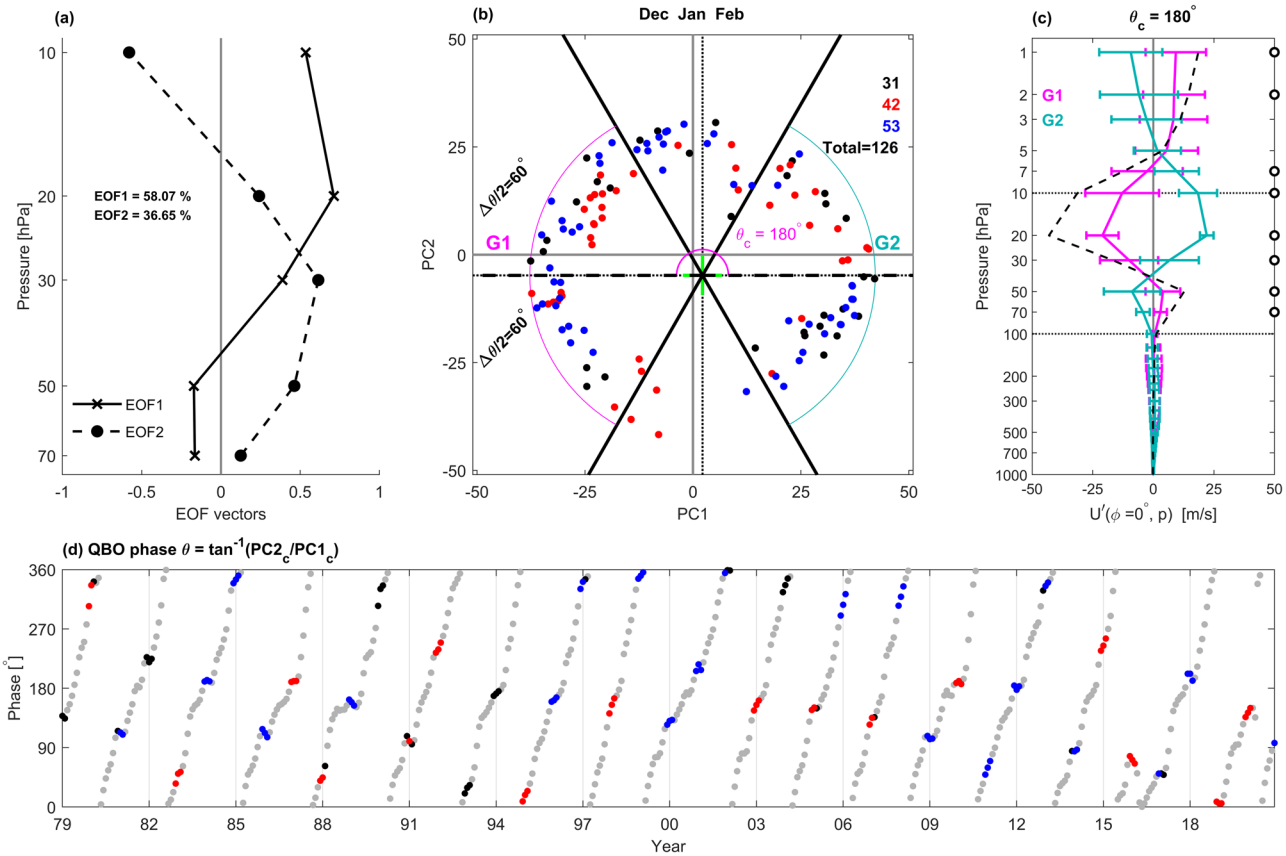

Fig. 1 | QBO representation in EOF phase space. a Vertical profiles of EOF1 (solid line) and EOF2 (dashed line). **b** Scatter plots in the *PC1* − *PC2* phase space for boreal winter months (DJF). Dots represent neutral (black), El Niño (red), and La Niña (blue) periods. The numbers of months for these periods are written at the top right corner with same color. The centroid of all the points is shown with a green + marker. The QBO phase angle is defined to be $\theta = \tan^{-1}\frac{PC2_c}{PC1_c}$, and $PC1_C$ and $PC2_C$ are defined with respect to the centroid point. Two data sample groups (G1 and G2) with opposite QBO phase are introduced for the central angle θ_c and half width $\Delta\theta/2$ (= ±60°). An example of G1 (pink circle arc) and G2 (light green arc) are shown for the central angle $\theta_c = 180°$. **c** Composite mean of the zonal mean zonal wind for G1 (pink) and G2 (light green) groups at $\theta_c = 180°$ with ± one standard deviations. The dashed profile shows the composite difference G1–G2, with circles on the right-hand side of the frame, indicating a statistically significant result (>95%) in the composite difference at the corresponding pressure levels. **d** Time variation of the QBO phase angle θ, where all months that are not DJF are shown with gray dots.

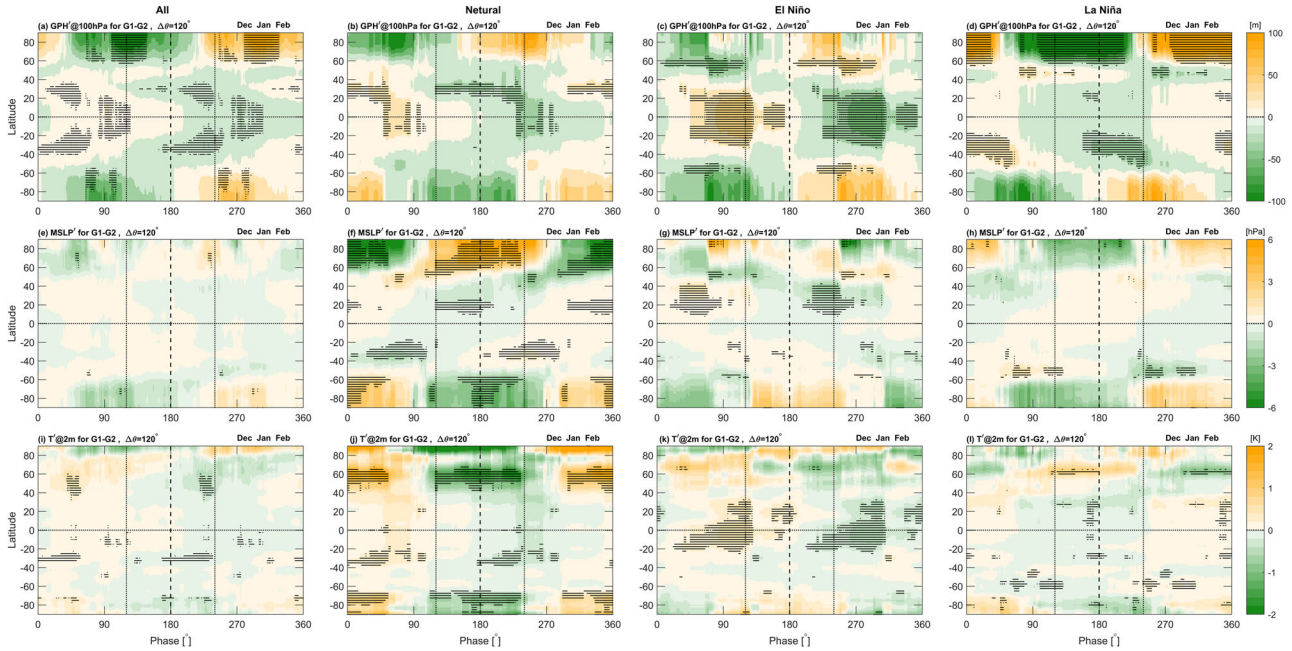

Fig. 2 | QBO phase angle versus latitude plots of composite difference G1–G2 for DJF for the following zonal mean quantities. a–d 100 hPa geopotential height anomalies (GPH′), **e–h** mean sea level pressure anomalies (MSLP′), and **i–l** surface temperature (T′) anomalies at 2 m height. From left to right, columns represent All, Neutral, El Niño, and La Niña periods. Black dots indicate regions with composite differences greater than 95% statistical significance. The vertical dotted line indicates the central phase angle $\theta_c = 180°$, with vertical dashed lines for θ_c 60°. Note that G1–G2 at $\theta_c = 180°$, is representative of QBO W − QBO E phase at 70 hPa and the reverse phase at 20 hPa (Fig. 1c).

investigating the effects of different phase combinations of ENSO and the QBO in determining NH winter surface climate.

Results

Zonal mean results

In order to study the influence of the QBO on NH surface weather during DJF, monthly zonal mean anomalies are calculated for (lower stratospheric) 100 hPa geopotential height (GPH′), mean sea level pressure (MSLP′), and surface temperature at 2 m (T′). The single prime superscript indicates deseasonalized anomalies, the departure from the climatological mean annual cycle in the 42-year data set (see Section "Data"). The zonal mean analysis is based on composite differences between the two groups G1 and G2 ($\theta_c \pm \frac{\Delta\theta}{2}$, and $\theta_c + 180° \pm \frac{\Delta\theta}{2}$, respectively) of QBO opposite phases, where θ_c is the central phase angle of the group and the averaging angle is $\Delta\theta = 120°$ (see Methods, Fig. 1b). A phase sweep of QBO central phase angle is performed, changing the phase every 1° in a complete cycle (0°–360°), to search the phase dependency for statistically significant effects. El Niño and La Niña periods were defined by when the Niño 3.4 monthly mean index exceeded ±0.4 K. These analyses were done separately for All, Neutral, El Niño, and La Niña groupings of monthly means (Fig. 2).

In the All category, significant negative differences of GPH′ anomalies at 100 hPa can be seen in the NH polar region (>60°N) for the phase angle range $100° < \theta_c < 140°$ (Fig.2a). These significant patterns are mainly contributed by La Niña (Fig. 2d), which exhibits more significant patterns in a wider phase domain ($70° < \theta_c < 210°$) with strong amplitude, and are absent for the neutral and El Niño periods (Fig. 2b, c). Significant patterns for La Niña are centered around the 135° phase angle, which represents a QBO westerly (W) wind maximum at 50 hPa (see, e.g., Fig.3 of ref. 26), where 50 hPa QBO W phase coincides with low geopotential height over the pole. This analysis confirms the finding of ref. 26, that the H-T mechanism is amplified during La Niña. Interestingly for neutral ENSO, all the variables exhibit systematic significant modulations simultaneously in the extratropical and polar regions for a broad phase range ($120° < \theta_c < 240°$) with centroid at 180° (vertical dashed line) (Fig. 2b, f, j). Note that the composite difference G1–G2 at centroid angle 180° is representative of QBO W – QBO E phase at 70 hPa and the reverse phase at 20 hPa (Fig. 1c). Significant negative anomalies of GPH′ at 100 hPa in the tropical to extratropical transition region (20°N−40°N) are associated with positive MSLP′ anomalies in the polar region (>50°N) and negative T′ at 2 m anomalies in the high latitude region (50°N−70°N). The significant anomalies in surface temperature extend up to 500 hPa (not shown).

These results suggest that it would be useful to explore the phase combination of neutral ENSO and centroid QBO phase angle 180° to better understand the joint QBO/ENSO influence on the NH high latitude surface via the tropical\extratropical UTLS. Figure 2g, h, k, l show that El Niño and La Niña interact with the QBO in a complex way to influence surface weather climate in the extratropical and polar regions. Considerations for interpretation include the modest sample size, uneven distribution of El Niño and La Niña events for QBO phases G1 and G2, and uneven distribution of strong El Niño or La Niña events in the particular QBO phase bins. It is also possible that there are significant longitudinal variations for a particular ENSO/QBO phase combination, but the zonal mean structure is not significantly modulated.

The present analysis focuses on neutral ENSO only at centroid angle 180°, for which G1 contains 10 months from five different winters and G2 contains 16 months from eight different winters. Using 1 month as a basic unit, and using a low threshold value (±0.4 K) for evaluating ENSO neutral, help to minimize ENSO bias for a particular phase of the QBO (G1 or G2).

Zonally asymmetric results for neutral ENSO

This analysis is extended for non-zonal components to explore the regional dependency of QBO modulation. Results are shown in NH polar orthographic projection in Fig. 3, for central phase angle $\theta_c = 180°$ during DJF and neutral ENSO. Top to bottom rows show 100 hPa GPH, MSLP, T at 2 m, and snow depth, respectively. The first column represents the 42-year DJF mean for neutral ENSO, while the second to fourth columns show composites of G1 anomalies, G2 anomalies, and their composite difference G1–G2, respectively.

During QBO W (G1, Fig. 3, second column) a 100 hPa ridge is amplified over the Bering Sea, near the base of the climatological Aleutian

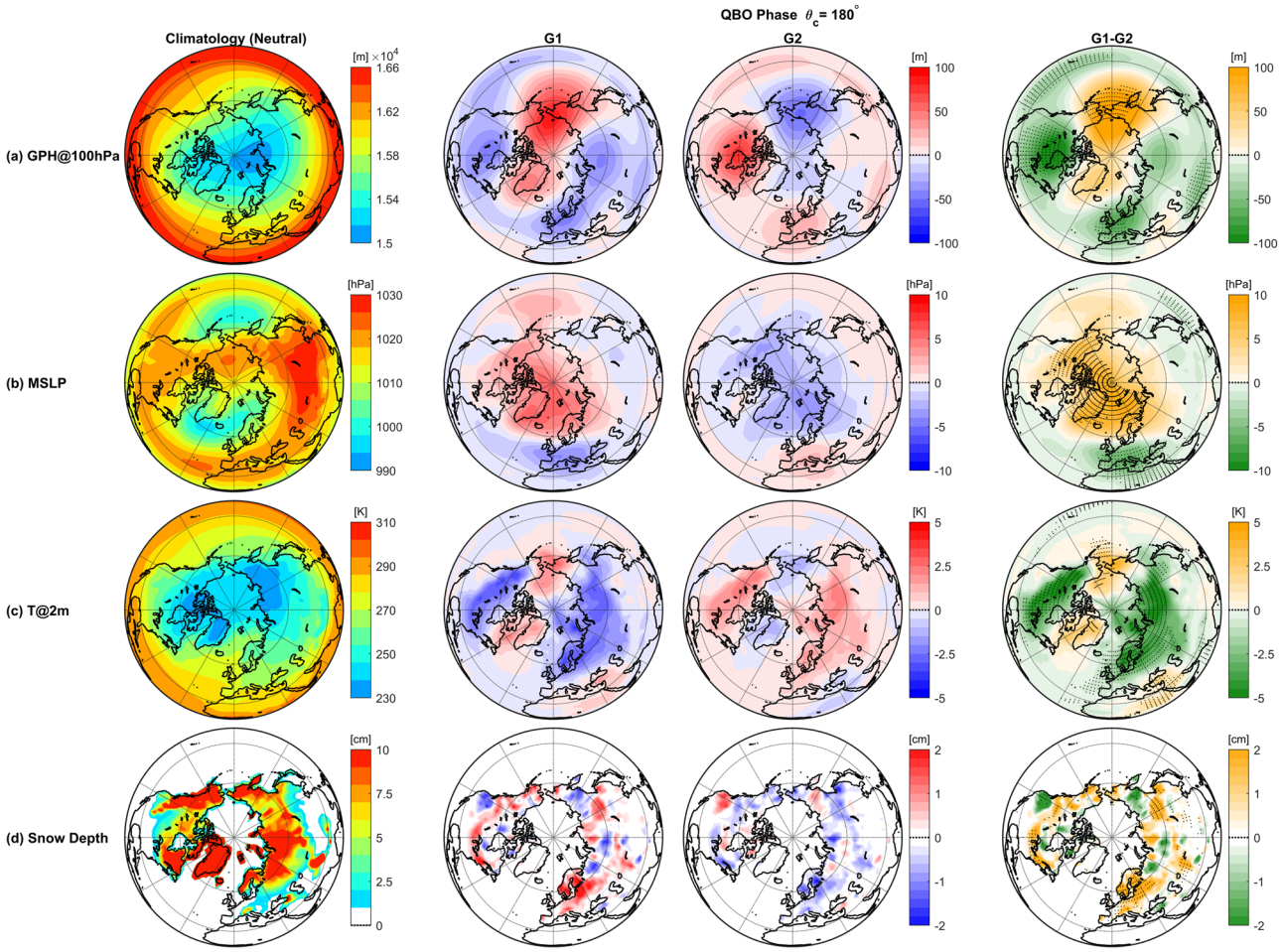

Fig. 3 | Northern Hemisphere orthographic polar projections (0°N–90°N) of. **a** 100 hPa GPH, **b** MSLP, **c** T at 2 m, and **d** snow depth at the central angle $\theta_c = 180°$ for a neutral ENSO period during DJF. The first, second, third, and fourth columns of each row represent the DJF climatological mean, composites of G1 anomalies (QBO W [E] at 70 hPa [20h Pa]), G2 anomalies (QBO E [W] at 70 hPa [20 hPa]), and their composite difference G1–G2 (QBO W [E]–E [W] at 70 hPa [20 hPa]), respectively. Black dots on the composite difference plots highlight regions where statistical significance exceeds 95%.

High[44], MSLP is higher over the Arctic, and the midlatitude continents are colder and snowier. During QBO E (G2, Fig. 3, third column) there is a somewhat different wave two anomaly pattern, with low 100 hPa heights over the Bering Sea, reduced MSLP over the Arctic, and the midlatitude continents are warmer and less snowy. The composite difference G1–G2 of GPH anomalies at 100 hPa shows a near wavenumber 2 pattern in the extratropical region (30°N–60°N) with significant negative anomalies across North America and southwestern Europe and (statistically insignificant) over Northern Russia (Fig. 3a, fourth column). The wavenumber 2 feature is present from 100 hPa to the boundary layer; and below the 100 hPa level the Northern Russia pattern becomes statistically significant. A significant positive anomaly in 100 hPa GPH′ lies over the Bering Sea. These results are consistent with the excitation of a weak NAM and more cold air outbreaks over the continents[28,32] during QBO W and neutral ENSO.

These composite difference patterns exhibit minor nonlinear features between G1 and G2, with stronger amplitude and a wider region for group G1. We hypothesize that the wavenumber 2 pattern may have been induced by the tropospheric pathway of QBO influence along the UTLS. In this connection, a significant positive pattern can be seen in MLSP′ as a semi-disc structure (150°W–60°E) from 60°N to the north pole, including North America, Greenland, Iceland, northern Europe, and the Norwegian Sea (Fig. 3b, fourth column). Significant negative patterns over southern Europe extend across the Mediterranean Sea and North Africa to the equator.

More robust features are seen in T′ at 2 m anomalies, with significant negative patterns over the Eurasian and North American sectors (Fig. 3c, fourth column), and simultaneously significant positive patterns spread across the northern Arabian Peninsula, part of eastern North Africa, and the Mediterranean Sea. Weakly significant positive patterns can also be observed near the Aleutian and Icelandic low-pressure systems. Similar patterns are found for snow depth anomaly over the both Eurasian and North American sectors, but with the opposite sign and smaller-scale features. Snow depth is higher when it is colder. The patterns of MLSP′, T′ at 2 m, and snow depth exhibit a linear transition from G1 to G2 with a marginally stronger amplitude for G1.

Regional dependence on QBO phase angle for neutral ENSO

In order to further investigate particular regions of interest, we analyzed the series for MSLP′ and T′ at 2 m against the QBO phase angle over selected domains which exhibited significant patterns for DJF during neutral ENSO (Fig. 3). The area of interest for MSLP′ is the significant region in the composite difference highlighted by the back dots over the positive golden color at the polar region, and over the negative dark green color at southwestern Europe (Fig. 3b, fourth column), and for T′ at 2 m the significant region of black dots over the negative dark green color at Eurasia, and North America (Fig. 3c, fourth column). A sine trigonometric function with mean amplitude defined from both groups (G1 and G2) is applied to each series. All resulting series with QBO phase are shown in Fig. 4, reflecting sinusoidal waves with phase constant 90° (dashed line).

As expected, the MSLP′ series over the Arctic and southwestern Europe have a phase difference of 180° because their significant patterns show the

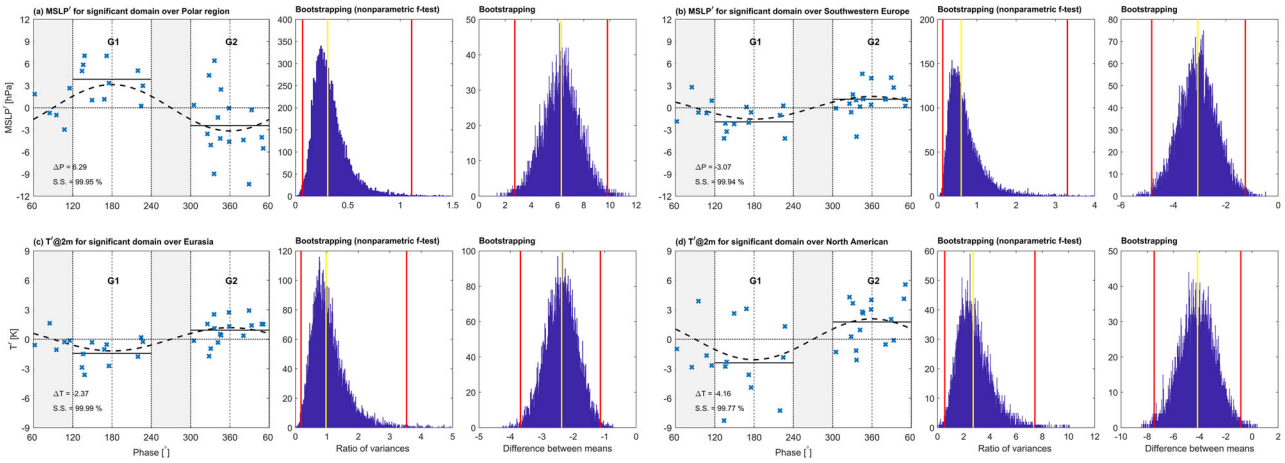

Fig. 4 | Regional anomalies (blue x's) of MSLP′ (top) and T′ at 2 m (bottom) as a function of QBO phase angle for statistically significant domains observed in non-zonal composite difference analysis at $\theta_c = 180°$ over. a the Polar region, **b** Southwestern Europe, **c** Eurasia, and **d** North America, during DJF and for neutral ENSO period. A sine trigonometric function with phase constant 90° is plotted as a black dashed line. Both opposite groups G1 and G2 at $\theta_c = 180°$ are highlighted with a white color background, while the transition phases between these two groups is highlighted with a light gray color background. The central vertical dotted line in each group G1 and G2 represents the central phase angle position of that group (i.e., $\theta_c = 180°$ for G1 and $\theta_c = 360°$ for G2), while the other two dotted vertical lines represent the boundaries of that group ($\theta_c \pm \frac{\triangle\theta}{2}$, $\triangle\theta = 120_\circ$ i.e., G1 ranges 120°−240° and G2 ranges 300°−60°). The horizontal black solid line denotes the mean value of all the data points within that group. One cycle of the QBO phase angle is plotted beginning at 60° so that both G1 and G2 are shown uninterrupted. The bootstrapping between G1 and G2 for each panel is shown with adjacent histogram plots on the right-hand side, with a total of 10,000 resample sizes. The first histogram is for nonparametric bootstrapping on the ratio of variance (*f*-test) for G1 and G2 and the second is for bootstrapping on the difference of the mean for G1 and G2. The region inside the two red vertical lines is at the 99% significant level.

opposite sign for composite differences (Fig. 3b, fourth column). The composite difference for MSLP between G1 and G2 is greater than 6 hPa (3 hPa) for the Arctic (southwestern Europe), and that for T′ at 2 m is greater than 2 K (4 K) for Eurasia (North America). The statistical significance of each difference series exceeds 99% for groups G1 and G2. Since the sampling is limited, we also used a bootstrap method with 10,000 resampling members to estimate the significance of G1 and G2. Results are shown in the adjacent histogram plots on the right-hand side of each series. The first histogram corresponds to nonparametric bootstrapping on the ratio of variance (f-test) for G1 and G2, and the second corresponds to bootstrapping on the difference of the means for G1 and G2. The yellow vertical line represents the original ratio of variance and difference of mean for G1 and G2 in the first and second histograms, respectively. The regions between the two red vertical lines lie at a 99% significant level. The significance is also met for the bootstrapping. The sinusoidal characteristics in the original sampling with QBO phase angle and the significance level in bootstrapping reflect the robustness of the results. These significant composite differences of MSLP′ and T′ at 2 m between the opposite QBO phases contain meaningful applications for seasonal and longer time-scale forecasts, although internal variations within each group are not also small.

Discussion

After confirming a consistent result with our previous study[26] that the H-T mechanism is amplified during the La Niña period, the present study investigates the QBO teleconnection with the boreal winter surface climate of NH mid and high latitudes regions in the presence and absence of El Niño and La Niña effects. A significant modulation of the climate dynamics governing surface anomalies is observed in the zonal mean and zonally asymmetric quantities for a specific QBO phase at the centroid angle of 180° for neutral ENSO period only (– 0.4 K <Niño 3.4 index <– 0.4 K). This specific QBO phase group G1 corresponds to maximum westerly wind at 70 hPa (QBO W) and simultaneously opposite easterly maximum at 20 hPa, whereas the G2 group (QBO E) has the opposite signs.

The QBO modulations of surface temperature and snow depth in Eurasia and North America illustrates a systematic association with MSLP in the Arctic region. High-pressure conditions over the polar region induce colder temperatures over the midlatitude continents and vice-versa. It is observed that ENSO neutral and QBO W favors a high value of MSLP (>6 hPa) over the polar region (>50°N), and cold conditions (~2–4 K) with high snow depth over Eurasia and North America, and the opposite effects during QBO E. A comparison of the anomaly patterns for QBO W and QBO E shows that the response is fairly linear, with marginally stronger amplitude for QBO W. During QBO W, anticyclonic anomalies are found at 100 hPa over the Bering Sea and the high North Atlantic. This favors higher arctic MSLP, especially in the North Atlantic. The pattern of colder surface temperatures extends farther into the midlatitudes, with enhanced snowfall farther south than normal, favoring a low-index NAM[23] and negative AO[31]. During QBO E, the Aleutian High and the trough over eastern North America at 100 hPa are reduced in amplitude such that the polar vortex is more zonally symmetric, with a region of lower MSLP over the pole. Such a high index NAM/AO flow confines polar air to higher latitudes, giving a warm anomaly across Eurasia and North America and reduced snow depth.

These results suggest that tropospheric wave activity is enhanced at high latitudes during QBO W and diminished during QBO E for the neutral ENSO period. This QBO pathway to the high latitude surface is independent of the traditional "stratospheric pathway" or H-T mechanism. To explore the hypothesis that there is enhanced planetary wave activity in the extratropical troposphere during QBO W for the neutral ENSO period, we investigate the joint effect of the QBO and ENSO on the Eliassen-Palm (EP) flux and flux divergence, which is shown in Fig. 5. In the DJF climatology there are two branches of EP fluxes, with some wave activity propagating upward in the troposphere near 40° N and refracting equatorward along the UTLS (Fig. 5, left column), and another branch propagating upward in the stratosphere near 60°N. A region of poleward flux of wave activity can also be observed along the UTLS from the equator to 15°N. It is difficult to discern any differences among the phases of ENSO in the climatology plots, although there are some differences in the shape of the zero-wind line of the zonal mean zonal wind in the lower stratosphere (Fig. 5a–c, left column). In climatology, one may also observe the vertical dipole of divergence/convergence of the EP flux (i.e., westerly/easterly wave drag) in the extratropical troposphere due to the baroclinic disturbances.

During QBO W and neutral ENSO the equatorward refraction of Rossby wave activity along the UTLS in the subtropics is diminished and the upward branch in the extratropical stratosphere is enhanced (Fig. 5a, G1),

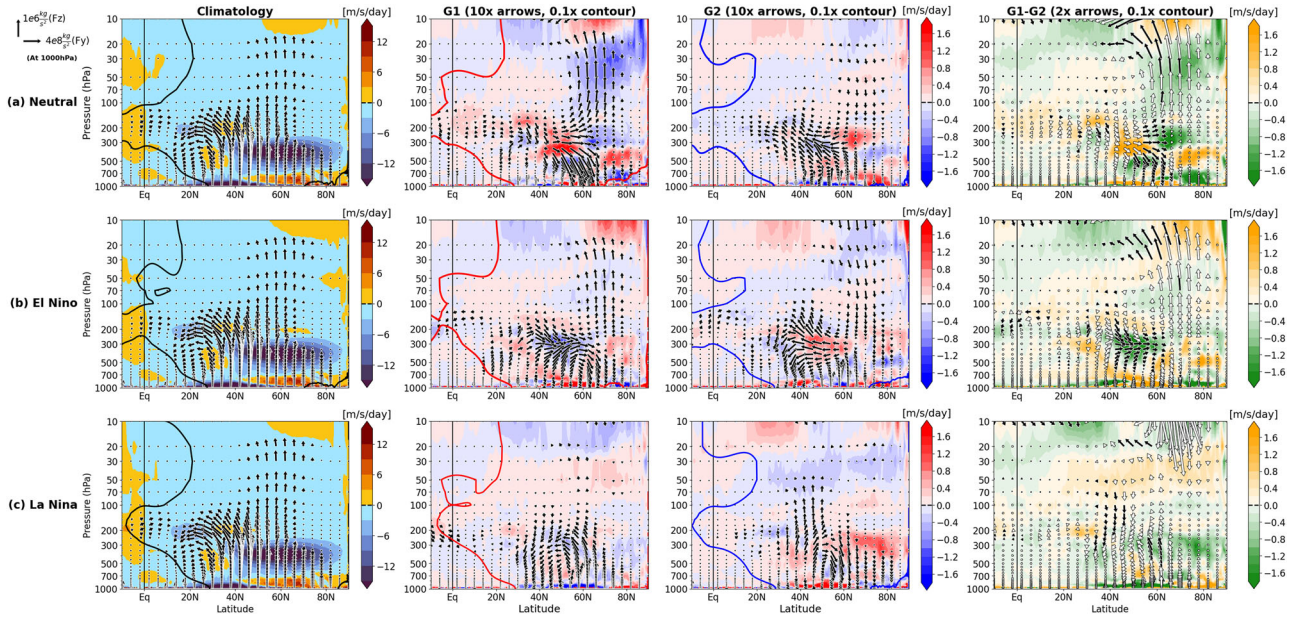

Fig. 5 | Latitude pressure sections of EP fluxes and EP flux divergence (color bar, m s^{-1} day^{-1}). a Neutral, **b** El Niño, and **c** La Niña, for the DJF climatological mean (first column), QBO phase group G1 (second column), QBO phase group G2 (third column), and G1–G2 (fourth column). G1(G2) corresponds approximately to QBO W (E) at 70 hPa. EP flux arrows are scaled by $\sqrt{p_o/p}$ in order to see features in the upper stratosphere. Reference vector lengths correspond to 10^6 kg s^{-2} (vertical) and 4×10^8 kg s^{-2} (meridional) at 1000 hPa. Black, red, and blue lines in the first, second, and third columns, respectively, are the zero-wind lines for zonal mean zonal wind for mean, G1, and G2, respectively. The vertical solid line in each plot denotes the position of the equator. Black arrows on the composite difference plots highlight regions where statistical significance exceeds 95%.

consistent with poleward confinement of wave activity and a higher amplitude wave two patterns in the lower stratosphere (Fig. 3a, G1). During QBO E, the equatorward branch along the UTLS is stronger and the upward branch in the extratropical stratosphere is diminished (Fig. 5a, G2). This pattern is more noticeable in their difference (Fig. 5a, G1–G2). These results are consistent with the high index NAM/AO patterns during QBO E and neutral ENSO shown in Fig.3.

In order to see the QBO route through the subtropical jets (STJs), the joint effect of the QBO and ENSO on the STJ is shown in Fig. 6. During neutral ENSO months (Fig. 6a), the amplified Aleutian High at 100 hPa during QBO W implies reduced westerlies across the Pacific and an equatorward shift in the STJ (Fig. 6a, G1), but in the Atlantic sector, an amplified Icelandic Low coincides with a stronger, northward-shifted STJ across the Mediterranean Sea. During QBO E and neutral ENSO (Fig. 6a, G2) the Pacific STJ is strengthened and zonal winds in the North Atlantic are stronger, consistent with a higher index NAM flow. During El Niño, the anomalies in G1 and G2 are diminished, but with similar difference patterns to neutral ENSO in the Atlantic and Eurasia (Fig. 6b), whereas QBO modulation is weak over the Pacific. During La Niña, the anomaly fields in G1, G2, and their difference show similar patterns to neutral ENSO, but with opposite signs and weaker amplitudes.

The joint effects of the QBO and ENSO on zonally asymmetric features of wind speed in the upper troposphere (Fig. 6) are consistent with the anomalies of EP flux and its divergence (Fig. 5).

These results suggest that, for neutral ENSO, when QBO anomalies of MMC, temperature, and zonal wind arrive in the UTLS, there is a QBO tropospheric pathway of influence via the subtropical UTLS towards high latitudes surface through wave-mean flow interaction[20], instead of through modulation of the polar vortex via the stratospheric pathway (H-T effect). In discussing possible mechanisms by which the QBO can influence the STJs, ref. 45 included changes in baroclinicity, eddy refraction, and changes in tropopause height. Although not yet fully understood, through the interaction among QBO anomalies, synoptic waves, and planetary waves, the tropospheric wave pattern is enhanced at high latitudes during QBO W, and is diminished during QBO E for neutral ENSO. This QBO teleconnection pathway through the STJs to the high latitude surface is independent of the traditional "stratospheric pathway" or H-T mechanism. Diagnosis of this pathway will provide valuable input to global circulation model simulations of internal sub-seasonal to seasonal variations, and can be implemented to improve long-range forecasting of these time scales over the Eurasian and North American areas.

Data and method

Data

ERA-5 reanalysis monthly mean data for the 42-year period 1979 to 2020 are used to analyze MSLP, T at 2 m, snow depth, horizontal winds (U, V), and geopotential height (GPH). The data are available at 37 pressure levels from 1000 hPa to 1 hPa. Due to development in model physics, core dynamics, and data assimilation, the ERA-5 data set offers several improvements over its predecessor (ERA-Interim)[46]. ERA-5 allows for the detailed evolution of weather systems as it outperforms the high-resolution regional analysis with a 31-km horizontal resolution[46]. The ENSO phase is defined based on the Niño 3.4 index in monthly mean data. The Hadley Centre Global Sea Ice and Sea Surface Temperature (HadISST) v1.1 data[47] is used to calculate the monthly Niño 3.4 index, which is defined as the de-seasonalized SST anomaly for the 42-year data set in the Pacific region 5°N–5°S, 120°W–170°W. Any month during the 42 years is considered to be during El Niño or La Niña whenever the Niño 3.4 index exceeds the threshold values ±0.4 K (+El Niño, – La Niña). All of the zonal and non-zonal analyses are performed at 2.5° spatial grid resolution.

Methods

QBO phase angle. The method of ref. 43 is used to represent the QBO in empirical orthogonal function (EOF) phase space for equatorial zonal mean zonal wind varying in altitude and time. The EOFs are obtained from the covariance matrix of the de-seasonalized stratospheric zonal mean zonal wind (U′) in the equatorial region at the five pressure levels 70, 50, 30, 20, and 10 hPa. The vertical structure of the first two leading EOFs is shown in Fig. 1a. These two functions explain 94.72% (58.07% plus 36.65%) of the total variance. EOF1 reflects the opposite phase of zonal wind in the upper

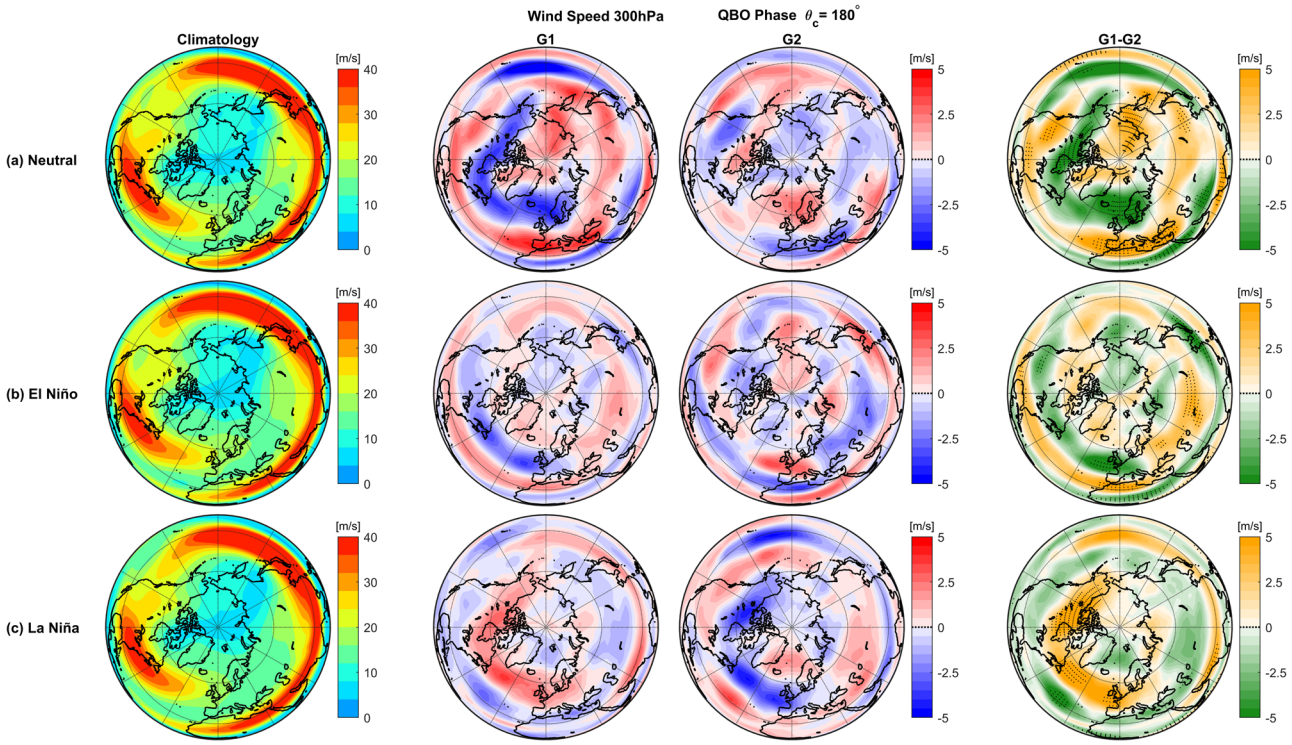

Fig. 6 | Northern Hemisphere orthographic polar projections (0°N–90°N) of wind speed at 300 hPa at the central angle $\theta_c = 180°$ during DJF. The first, second, third, and fourth columns of each row represent the DJF climatological mean, composites of G1 anomalies, composites of G2 anomalies, and their composite difference G1–G2, respectively. From top to bottom, rows are for **a** Neutral, **b** El Niño, and **c** La Niña. Black dots on the composite difference plots highlight the regions where statistical significance exceeds 95%.

(<50 hPa, positive) and lower (>50 hPa, negative) stratosphere, while EOF2 reflects maximum zonal wind in the mid-stratosphere (around 30 hPa, positive). A scatter plot of the first two principal components (*PC*1 and *PC*2) associated with these two EOFs is shown in Fig. 1b (for DJF only). The QBO phase angle is defined as $\theta = \tan^{-1}\frac{PC2_c}{PC1_c}$, where $PC1_c$ and $PC2_c$ are defined with respect to the locus of the centroid (Cx, Cy) of all months for 42 years (shown as a + green marker in Fig. 1b) i.e., $PC1_c = PC1 - Cx$, and $PC2_c = PC2 - Cy$. The centroid is determined numerically (2.22, –4.79) to minimize the variance of the distance to all points for the whole data period. Successive progression of the QBO-phase angle θ can be seen with time (Fig. 1d) except for the disturbed periods 2015/2016 and 2019/2020. As introduced by ref. 26, this study uses the same composite difference analysis for a central angle θ_c between two groups G1 and G2 of QBO opposite phases ($\theta_c \pm \frac{\Delta\theta}{2}$, and$\theta_c + 180° \pm \frac{\Delta\theta}{2}$, respectively, $\Delta\theta = 120°$), and also gives weight to the phase transition between these two opposite groups (i.e., 60° between G1 and G2 and 60° between G2 and G1). Therefore, the composite difference analysis will neglect the phase transition between two opposite phases of the QBO. As an example, G1 and G2 are shown, along with a dashed line at the central angle θ_c = 180° (Fig. 1b). Most results are shown for groups G1 and G2 with central angle θ_c = 180° (Fig. 1b, c), for which G1 corresponds to the QBO W phase at 50 to 70 hPa, and G2 corresponds to QBO E phase at 50 to 70 hPa with a clear separation between these two phases at 70 hPa, and simultaneously the opposite phase at 20 hPa (Fig. 1c). Using individual months, the statistical significance of the composite difference is evaluated using a two-sided Student's *t*-test, assuming two independent samples in each G1 and G2 group. All results for composite difference patterns are discussed at the 95% significant level. Further, to avoid monthly intra-seasonal variability within a group, de-seasonalized anomalies are used for the composite difference analysis. A single superscript prime on any variable, X′, represents the de-seasonalized anomaly, i.e., its deviation from the 42-year (1979–2020) climatological mean annual cycle.

EP flux and divergence. The EP flux[48] is a diagnostic tool for assessing wave propagation and wave-mean flow interaction. It is a vector representation for the propagation of synoptic and planetary Rossby wave activity in the meridional plane. An upward component indicates a poleward heat flux while an equatorward component indicates a poleward momentum flux. EP flux divergence implies a source of Rossby wave activity, and EP flux convergence implies absorption of Rossby wave activity. EP flux divergence represents the body force, or net effect of waves on the zonal mean zonal wind, with EP flux convergence causing deceleration of zonal mean westerlies and EP flux divergence causing acceleration. The primary effect of a region of EP flux convergence, however, is to induce poleward motion, with an associated MMC and quadrupole of temperature anomalies in the meridional plane (warm over cold in the tropics and cold over warm at high latitudes) associated with adiabatic vertical motions.

The meridional and vertical components of the EP flux are calculated in pressure coordinates using the following expressions[49,50]:

$$f_\phi = -\overline{u'v'} + \overline{u}_p\frac{\overline{u'\theta'}}{\overline{\theta}_p}, f_p = \left(f - \frac{1}{a\cos\phi}\frac{\partial(\overline{u}\cos\phi)}{\partial\phi}\right)\frac{\overline{v'\theta'}}{\overline{\theta}_p} - \overline{u'w'},$$

and

$$F = \left(F_\phi, F_p\right) = \rho a\cos\phi\,(f_\phi, f_p),$$

where ϕ is latitude, p pressure, u zonal wind, v meridional wind, w vertical wind, θ potential temperature, $f = 2\,\Omega\sin\phi$ is the Coriolis parameter, Ω is the angular frequency of Earth's rotation, a denotes the Earth's radius, and $\rho\,(p)$ is mean density. The zonal mean is indicated with an overbar; a prime denotes a departure from the zonal mean. Potential temperature is calculated from $\theta = T(\frac{P_0}{P})^\kappa$ and density from $\rho = \rho_0\frac{P}{P_0}$. The EP flux divergence is

calculated from $\vec{\nabla} \cdot \vec{F} = \frac{1}{\rho a \cos\phi}\frac{\partial(\cos\phi F_\phi)}{\partial\phi} + \frac{1}{\rho a \cos\phi}\frac{\partial(F_p)}{\partial p}$. Twice daily (0000 and 1200 UTC) ERA-5 analyses are used for calculating EP fluxes and then monthly mean averages are constructed. EP flux arrows are scaled by $\sqrt{p_o/p}$ in order to see features in the upper stratosphere.

Data availability

All data used in this study are openly accessible for the public. The ERA-5 data set is available online at https://cds.climate.copernicus.eu/cdsapp#!/home. The HadISST data set is available at https://www.metoffice.gov.uk/hadobs/hadisst/data/download.html. The EP fluxes data are archived in Zenodo (https://doi.org/10.5281/zenodo.10140775[51])

Code availability

All programming codes to generate the figures in this paper are available with the corresponding author, Vinay Kumar, and can be provided on request.

Received: 12 December 2023; Accepted: 25 April 2024;
Published online: 11 May 2024

References

1. Charney, J. G. & Drazin, P. G. Propagation of planetary-scale disturbances from the lower into the upper atmosphere. *J. Geophys. Res.* **66**, 83–109 (1961).
2. Andrews, D. G. Wave, mean-flow interaction in the middle atmosphere. *Adv. Geophys.* **28A**, 249–275 (1985).
3. Liebmann, B. & Hartmann, D. L. Interannual variations of outgoing IR associated with tropical circulation changes during 1974-78. *J. Atmos. Sci.* **39**, 1153–1162 (1982).
4. Linkin, M. E. & Nigam, S. The North Pacific oscillation–West Pacific teleconnection pattern: mature-phase structure and winter impacts. *J. Clim.* **21**, 1979–1997 (2008).
5. Budikova, D., Ford, T. W. & Wright, J. D. Characterizing winter season severity in the Midwest United States, part II: interannual variability. *Int. J. Climatol.* **42**, 3499–3516 (2022).
6. Trenberth, K. E. The definition of El Niño. *Bull. Am. Meteorol. Soc.* **78**, 2771–2778 (1997).
7. Baldwin, M. P. et al. The quasi-biennial oscillation. *Rev. Geophys.* **39**, 179–229 (2001).
8. Horel, J. D. & Wallace, J. M. Planetary-scale atmospheric phenomena associated with the southern oscillation. *Mon. Weather Rev.* **109**, 813–829 (1981).
9. van Loon, H. & Labitzke, K. The southern oscillation part V: the anomalies in the lower stratosphere of the Northern Hemisphere in winter and a comparison with the quasi-biennial oscillation. *Mon. Weather Rev.* **115**, 357–369 (1987).
10. Ropelewski, C. F. & Halpert, M. S. North American precipitation and temperature patterns associated with the El Niño/Southern Oscillation (ENSO). *Mon. Weather Rev.* **114**, 2352–2362 (1986).
11. Higgins, R. W., Leetmaa, A. & Kousky, V. E. Relationships between climate variability and winter temperature extremes in the United States. *J. Clim.* **15**, 1555–1572 (2002).
12. Lee, S., Park, H. S., Song, S. Y. & Yeh, S. W. Distinct impacts of two types of El Niño events on northern winter high-latitude temperatures simulated by CMIP6 climate models. *Environ. Res. Lett.* **18**, 034035 (2023).
13. Ineson, S. & Scaife, A. The role of the stratosphere in the European climate response to El Niño. *Nat. Geosci.* **2**, 32–36 (2009).
14. Luo, B. H., Luo, D. H., Dai, A. G., Simmonds, I. & Wu, L. A connection of winter Eurasian cold anomaly to the modulation of Ural blocking by ENSO. *Geophys. Res. Lett.* **48**, e2021GL094304 (2021).
15. Butler, A. H., Polvani, L. M. & Deser, C. Separating the stratospheric and tropospheric pathways of El Niño Southern Oscillation teleconnections. *Environ. Res. Lett.* **9**, 024014 (2014).
16. Domeisen, D. I. V. & Butler, A. H. Stratospheric drivers of extreme events at the Earth's surface. *Commun. Earth Environ.* **1**, 59 (2020).
17. Scaife, A. A. et al. Predictability of the Quasi-Biennial oscillation and its northern winter teleconnection on seasonal to decadal timescales. *Geophys. Res. Lett.* **41**, 1752–1758 (2014).
18. Gray, W. M., Scheaffer, J. D. & Knaff, J. A. Influence of the stratospheric QBO on ENSO variability. *J. Meteorol. Soc. Jpn.* **70**, 975–995 (1992).
19. Collimore, C. C., Martin, D. W., Hitchman, M. H., Huesmann, A. & Waliser, D. E. On the relationship between the QBO and tropical deep convection. *J. Clim.* **16**, 2552–2568.975 (2003).
20. Garfinkel, C. I. & Hartmann, D. L. The influence of the quasi-biennial oscillation on the troposphere in winter in a hierarchy of models. Part I: simplified dry GCMs. *J. Atmos. Sci.* **68**, 1273–1289 (2011).
21. Haynes, P. et al. The influence of the stratosphere on the tropical troposphere. *J. Meteorol. Soc. Jpn.* **99**, 803–845 (2021).
22. Yoden, S., Kumar, V., Dhaka, S. K. & Hitchman, M. H. Global monsoon systems and their modulation by the equatorial Quasi-Biennial oscillation. *MAUSAM* **74**, 239–252 (2023).
23. Thompson, D. W. J. & Wallace, J. M. Annular modes in the extratropical circulation Part I. Month-to-month variability. *J. Clim.* **13**, 1000–1016 (2000).
24. Garfinkel, C. I. & Hartmann, D. L. Different ENSO teleconnections and their effects on the stratospheric polar vortex. *J. Geophys. Res.* **113**, D18114 (2008).
25. Hu, J., Li, T., Xu, H. & Yang, S. Lessened response of boreal winter stratospheric polar vortex to El Niño in recent decades. *Clim. Dyn.* **49**, 263–278 (2017).
26. Kumar, V., Yoden, S. & Hitchman, M. H. QBO and ENSO effects on the mean meridional circulation, polar vortex, subtropical westerly jets, and wave patterns during boreal winter. *J. Geophys. Res. Atmos.* **127**, e2022JD036691 (2022).
27. Gray, L. J. et al. Surface impacts of the Quasi Biennial oscillation. *Atmos. Chem. Phys.* **18**, 8227–8247 (2018).
28. Hitchman, M. H., Yoden, S., Haynes, P. H., Kumar, V. & Tegtmeier, S. An observational history of the direct influence of the stratospheric quasi-biennial oscillation on the tropical and subtropical upper troposphere and lower stratosphere. *J. Meteorol. Soc. Jpn.* **99**, 239–267 (2021).
29. Holton, J. R. & Tan, H.-C. The influence of the equatorial quasi-biennial oscillation on the global circulation at 50 mb. *J. Atmos. Sci.* **37**, 2200–2208 (1980).
30. Holton, J. R. & Tan, H.-C. The quasi-biennial oscillation in the Northern Hemisphere lower stratosphere. *J. Meteorol. Soc. Jpn.* **60**, 140–147 (1982).
31. Thompson, D. W. J. & Wallace, J. M. The Arctic oscillation signature in the wintertime geopotential height and temperature fields. *Geophys. Res. Lett.* **25**, 1297–1300 (1998).
32. Thompson, D. W. J., Baldwin, M. P. & Wallace, J. M. Stratospheric connection to Northern Hemisphere wintertime weather: Implications for prediction. *J. Clim.* **15**, 1421–1428 (2002).
33. Taguchi, M. Observed connection of the stratospheric quasi biennial oscillation with El Nino-Southern Oscillation in radiosonde data. *J. Geophys. Res.* **115**, D18120 (2010).
34. Yuan, W., Geller, M. A. & Love, P. T. ENSO influence on QBO modulations of the tropical tropopause. *Q. J. Roy. Meteorol. Soc.* **140**, 1670–1676 (2014).
35. Zhou, T. et al. Exploring the ENSO modulation of the QBO periods with GISS E2.2 models. *Atmos. Chem. Phys.* **24**, 509–532 (2024).
36. Hansen, F., Matthes, K. & Wahl, S. Tropospheric QBO–ENSO interactions and differences between the Atlantic and Pacific. *J. Clim.* **29**, 1353–1368 (2016).
37. Wei, K., Chen, W. & Huang, R. Association of tropical Pacific sea surface temperatures with the stratospheric Holton-Tan oscillation in the Northern Hemisphere winter. *Geo. Res. Lett.* **34**, L16814 (2007).

38. Ma, T., Chen, W., An, X., Garfinkel, C. I. & Cai, Q. Nonlinear effects of the stratospheric quasi-biennial oscillation and ENSO on the North Atlantic winter atmospheric circulation. *J. Geo. Res. Atmos.* **128**, e2023JD039537 (2023).
39. Kidston, J. et al. Stratospheric influence on tropospheric jet streams, storm tracks and surface weather. *Nat. Geosci.* **8**, 433–440 (2015).
40. Cai, Q., Chen, W., Chen, S., Ma, T. & Garfinkel, C. I. Influence of the quasi-biennial oscillation on the spatial structure of the wintertime Arctic Oscillation. *J. Geophys. Res. Atmos.* **127**, e2021JD035564 (2022).
41. Butchart, N. The stratosphere: a review of the dynamics and variability. *Weather Clim. Dynam.* **3**, 1237–1272 (2022).
42. Anstey, J. A. et al. Impacts, processes and projections of the quasi-biennial oscillation. *Nat. Rev. Earth Environ.* **3**, 588–603 (2022).
43. Wallace, J. M., Panetta, R. L. & Estberg, J. Representation of the equatorial stratospheric quasi-biennial oscillation in EOF phase space. *J. Atmos. Sci.* **50**, 1751–1762 (1993).
44. Harvey, V. L. & Hitchman, M. H. A climatology of the Aleutian high. *J. Atmos. Sci.* **53**, 2088–2101 (1996).
45. Wang, J., Kim, H.-M. & Chang, E. K. M. Interannual modulation of Northern Hemisphere winter storm tracks by the QBO. *Geo. Res. Lett.* **45**, 2786–2794 (2018).
46. Hersbach, H. et al. The ERA5 global reanalysis. *Q. J. R. Meteorol. Soc.* **146**, 1999–2049 (2020).
47. Rayner, N. A. et al. Global analyses of sea surface temperature, sea ice, and night marine air temperature since the late nineteenth century. *J. Geophys. Res. Atmos.* **108**, 4407 (2003).
48. Eliassen, A. & Palm, T. On the transfer of energy in stationary mountain waves. *Geofysiske publikasjoner* **22**, 1–23 (1960).
49. Andrews, D. G., Mahlman, J. D. & Sinclair, R. W. Eliassen- Palm diagnostics of wave-mean flow interaction in the GFDL "SKYHI" general circulation model. *J. Atmos. Sci.* **40**, 2768–2784 (1983).
50. Jucker, M. Scaling of Eliassen-Palm flux vectors. *Atmos. Sci. Lett.* **22**, e1020 (2021).
51. Du, W. & Hitchman M. H. Monthly mean Eliassen-Palm fluxes and EP flux divergences for boreal winter months (Dec-Jan-Feb) from 1979 to 2020 using ERA5 data (Data set). *Zenodo* https://doi.org/10.5281/zenodo.10140775 (2023).

Acknowledgements

The authors would like to thank all members of the ERA-5 reanalysis, and HadISST teams for providing the data sets. M.H.H. was supported by NSF grant AGS 1947658.

Author contributions

V.K. and S.Y. jointly worked on the research design and methodology. V.K. analyzed the data and wrote the first draft of the paper. M.H.H. and W.D. jointly performed the analysis for EP flux. M.H.H. contributed significantly to the discussion section. M.H.H., W.D., S.K.D., and S.Y. contributed to the conceptualization, review, and edited the draft.

Competing interests

The authors declare no competing interests.

Additional information

Supplementary information The online version contains supplementary material available at https://doi.org/10.1038/s43247-024-01422-7.

Correspondence and requests for materials should be addressed to Vinay Kumar.

Peer review information *Communications Earth & Environment* thanks the anonymous reviewers for their contribution to the peer review of this work. Primary Handling Editors: Mengze Li, Heike Langenberg. A peer review file is available.